

1995 CEDAR WORKSHOP
Boulder, Colorado
June 26-30, 1995

Tutorial Lecture

by Gary E. Thomas
University of Colorado

**Global Change in the
Mesosphere-Lower thermosphere (MLT) Region:
Has it already arrived?**

Topics

- Climate Change:
 - in Troposphere
 - in Mesosphere and Lower Thermosphere
 - Evidence from NLC occurrence changes
 - Possible MLT cooling, Na-D layer lowering
- Response of MLT to dynamical and chemical forcing
 - Heating/cooling at summer mesopause
 - Temperature and winds
- Mesospheric Clouds (MC)
 - MC secular changes
 - Methane hypothesis
 - Temperature hypothesis
 - Ice particle microphysics
- Modeling of the MLT
 - 1D and 2D modeling results
 - CO_2 , CH_4 doubling/halving experiments
 - MC existence region changes
- Recent results and conclusions

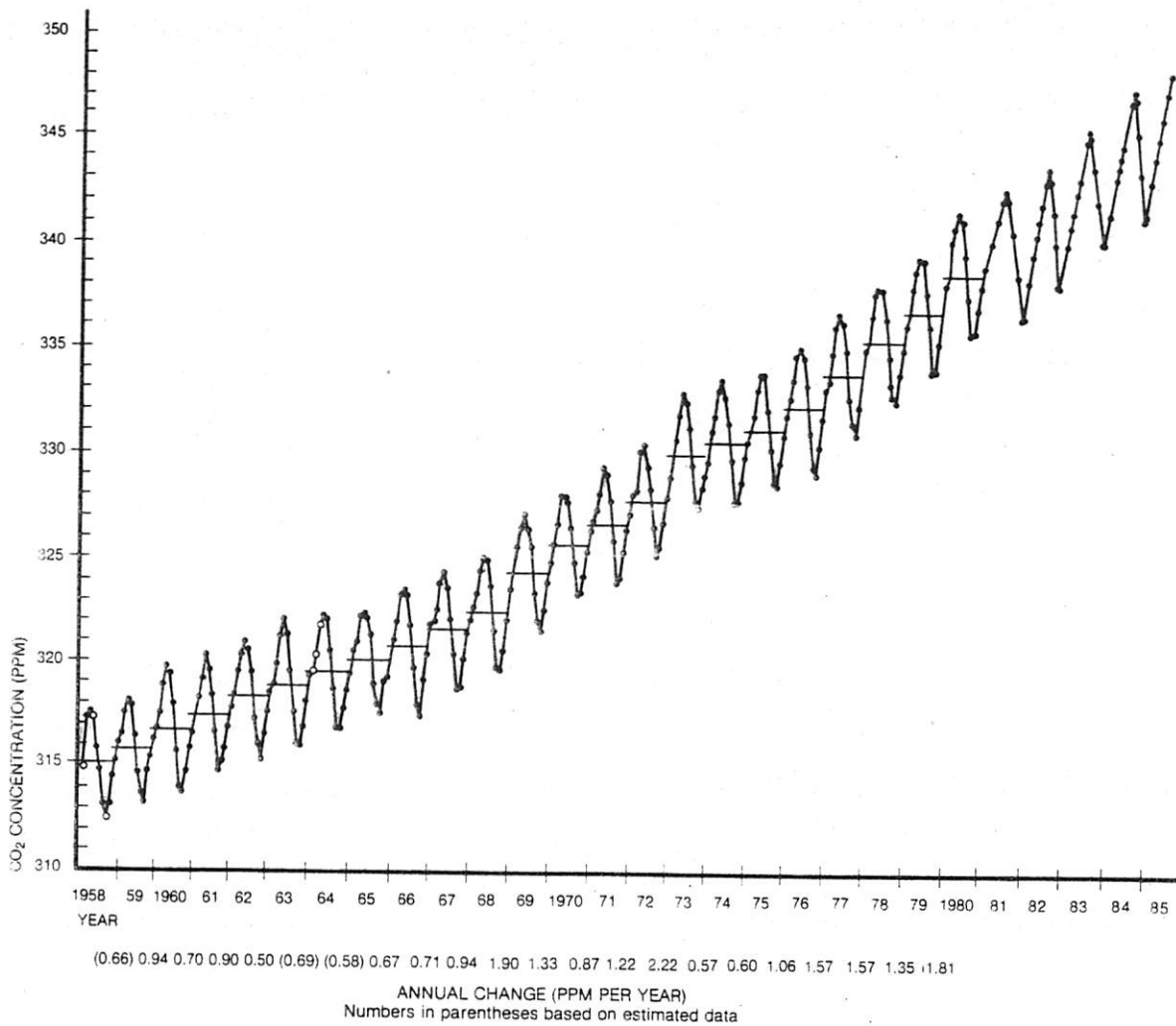


FIGURE 18.16

Upward trend in atmospheric carbon dioxide levels as measured at Mauna Loa Observatory, Hawaii. Horizontal lines represent average annual values. Open circles are estimated values. [Data from C. D. Keeling et al. Scripps Institution of Oceanography, as reported in M. C. MacCracken, and H. Moses. "The First Detection of Carbon Dioxide Effects: Workshop Summary." *Bulletin of the American Meteorological Society* 63 (1982):1165.]

the growing season because of photosynthetic removal and recover thereafter. This annual cycle is superimposed on a nearly exponential rate of growth: the rate of carbon dioxide increase rose from about 0.7 ppm (parts per million) per year in 1958 to about 1.8 ppm per year in 1981. In the ten years prior to 1986, the total global CO₂ content increased by 4.6 percent. Sketchy data

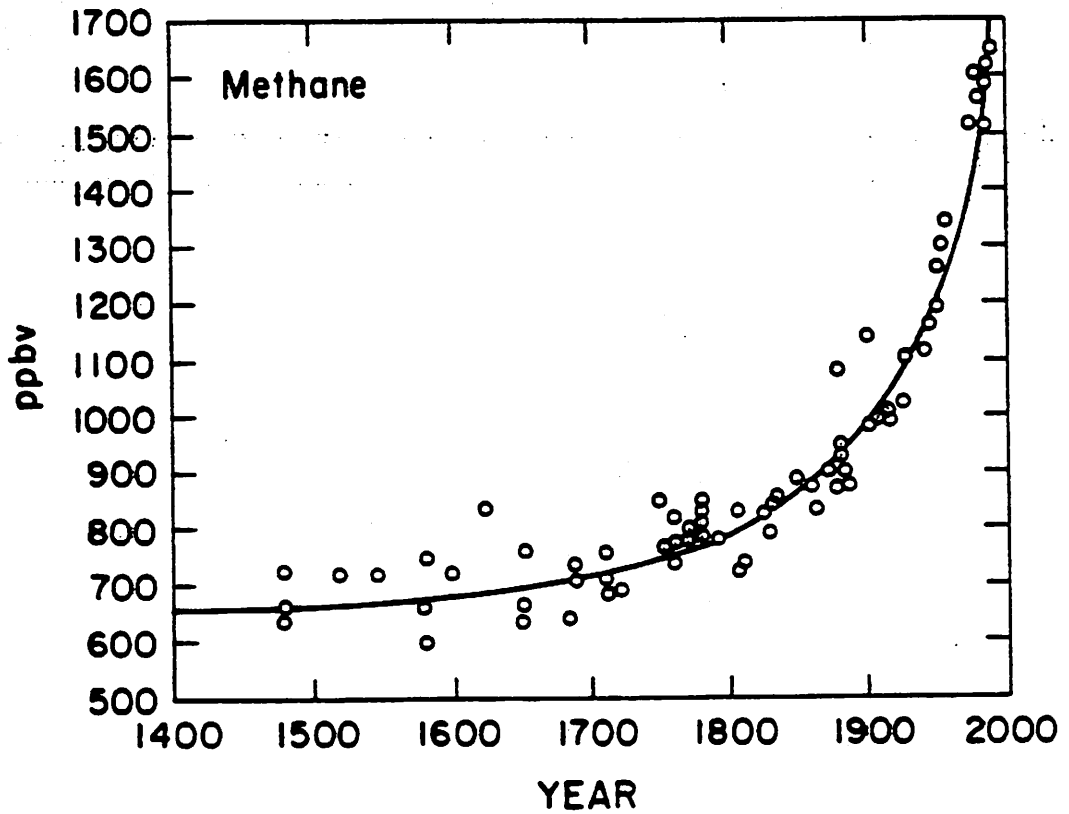
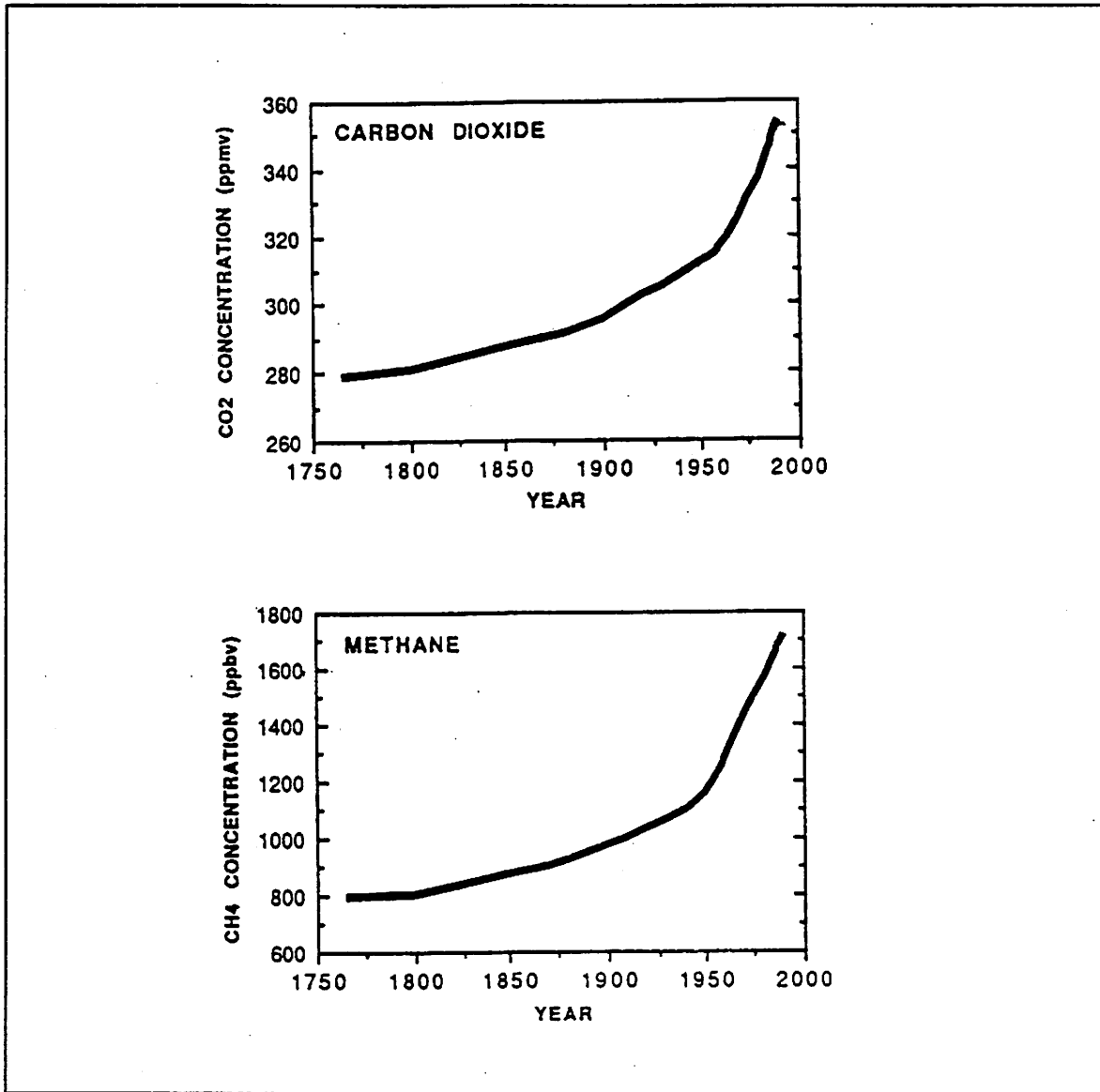
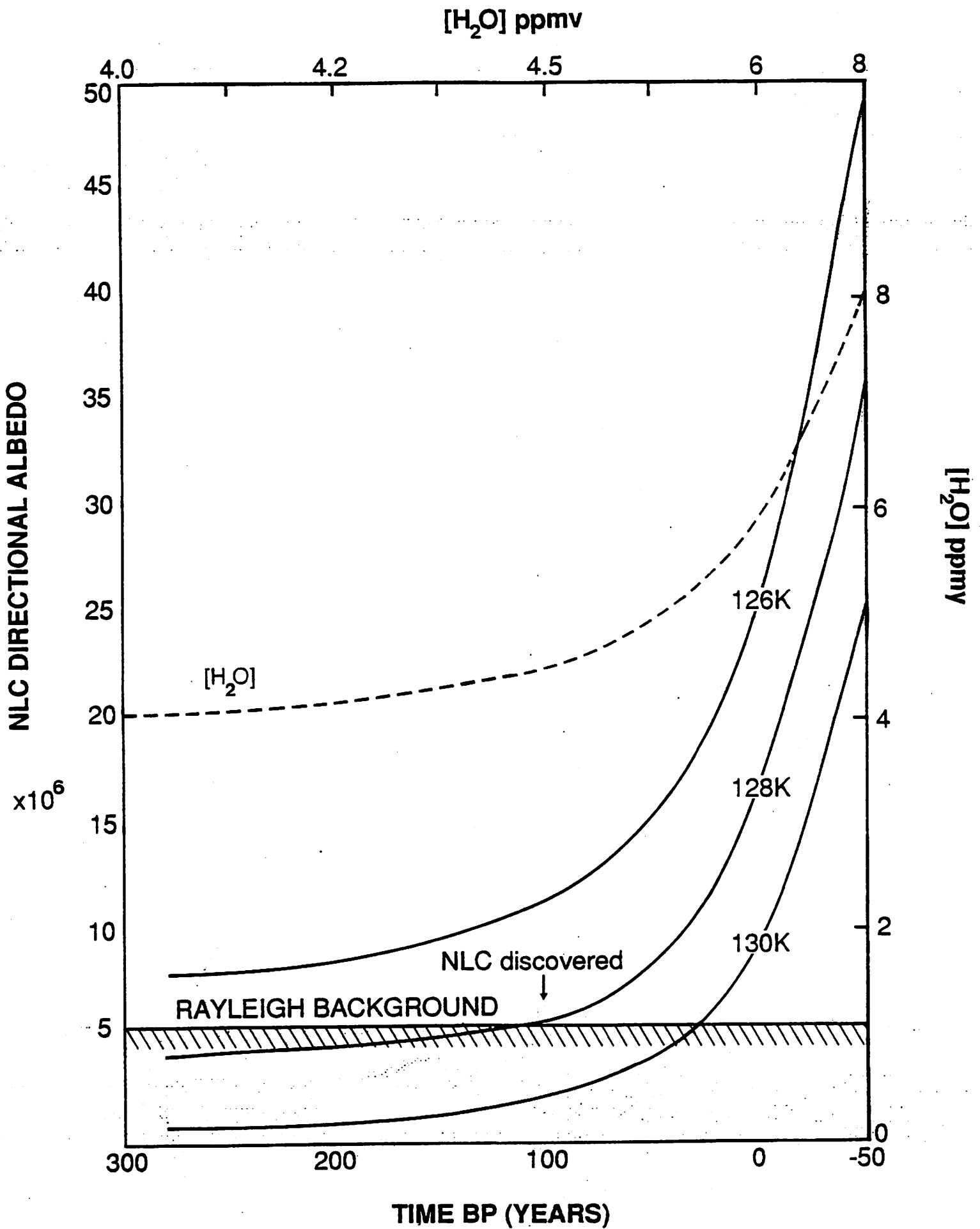


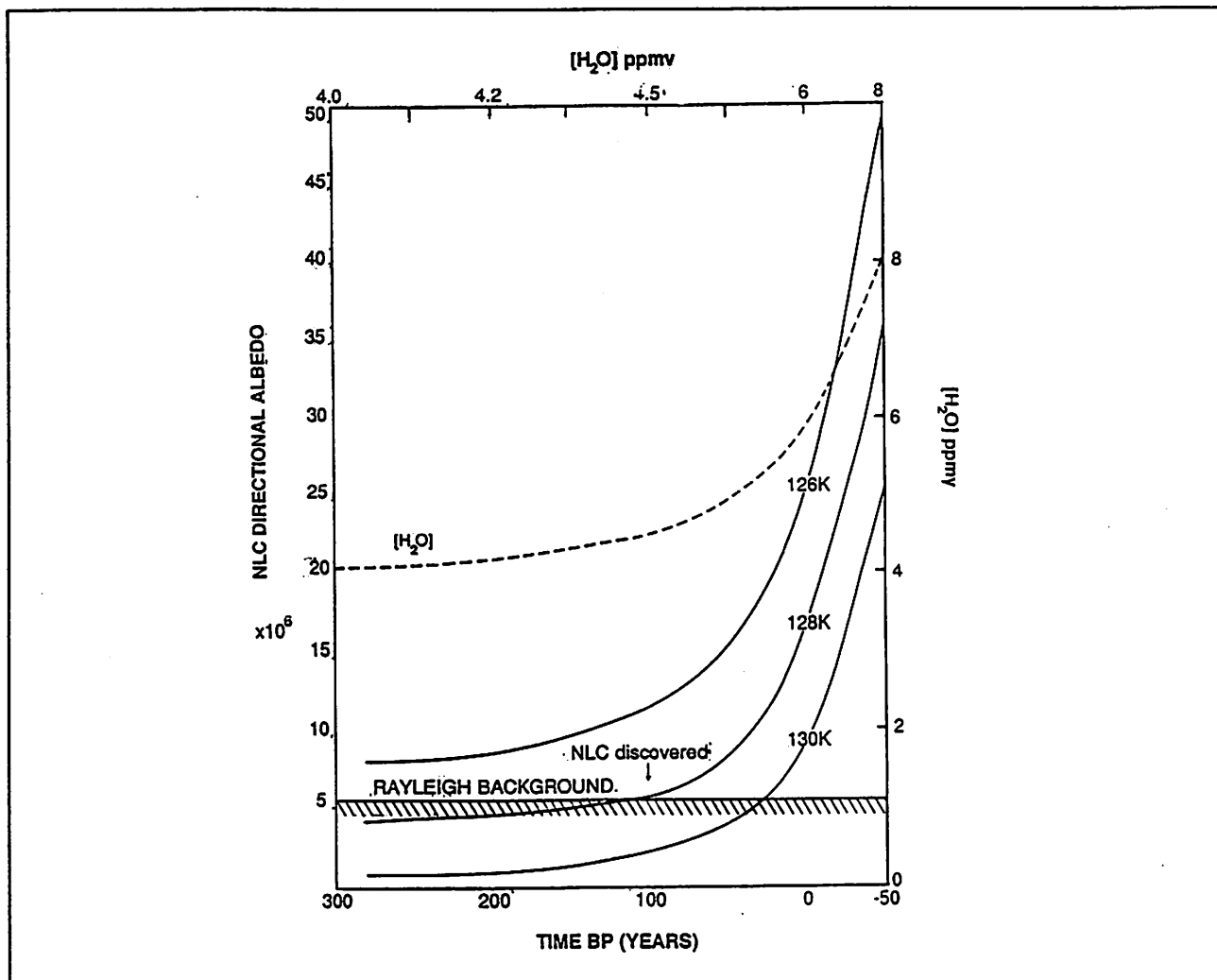
Figure 15. The concentration of methane in the atmosphere at various times in the past as deduced from measurements of air trapped in ice cores (1480–1950) and from direct measurements of air samples (after 1950). The concentration is plotted in parts per billion by volume. From John Firor, *The Changing Atmosphere: A Global Challenge*. Yale University Press, 1990. Reprinted by permission.



Concentrations of CO_2 and CH_4 have risen sharply over the past 150 years. From *Climate Change: the IPCC Scientific Assessment*, ed. Houghton, Jenkins and Ephraums, 1991.

- These increases have resulted from:
 - Industrial emissions
 - Intensification of agricultural practises
 - Development of transportation

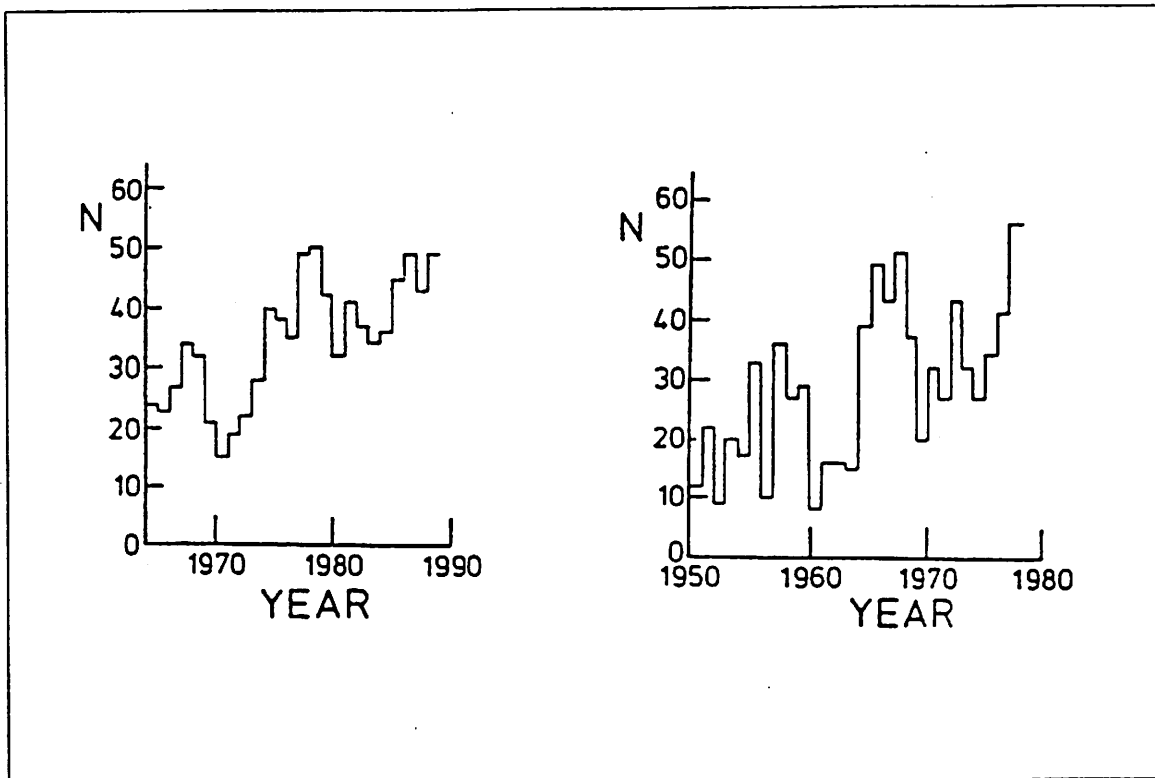




Noctilucent Clouds - Are they a recent phenomenon?

- Reference: G. E. Thomas et al, Relation between increasing methane and the presence of ice clouds at the mesopause, *Nature*, **338**,490-492,1989
- The nearly-doubling of CH_4 would have caused a 25% increase in upper atmospheric H_2O .
- Jensen model* predicts a ten-fold increase in cloud brightness, due to this change in H_2O .

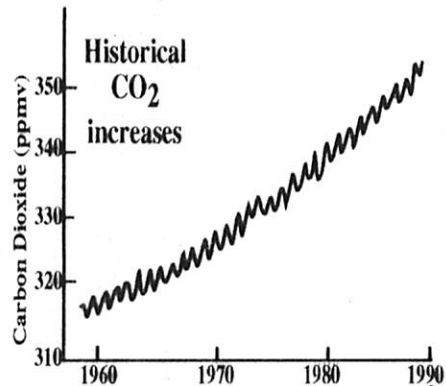
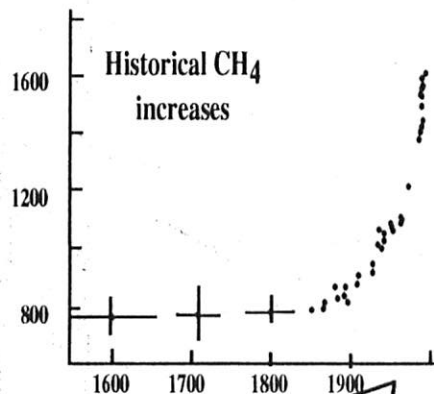
* Jensen, E. J., *A Numerical Model of Polar Mesospheric Cloud Formation and Evolution*, PhD Thesis, Univ. of Colorado, 1989



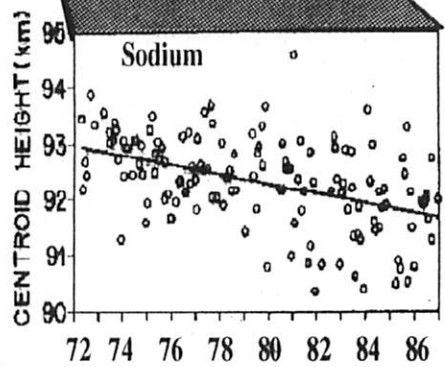
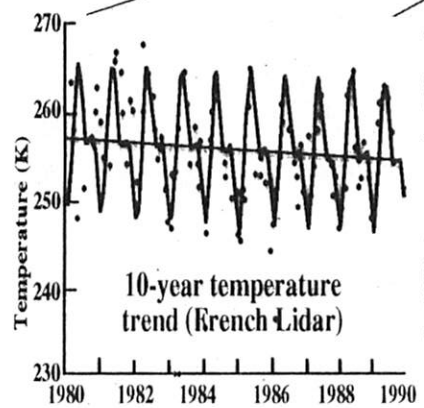
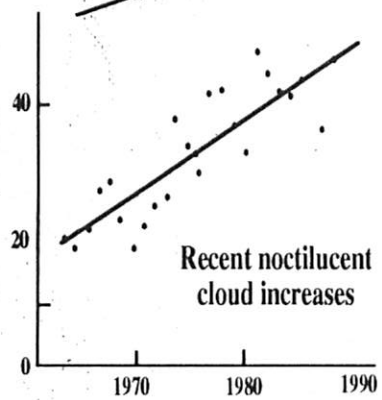
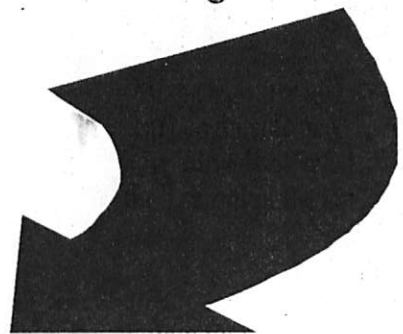
- (left) Plot of the number of nights per year, N , on which NLC's were reported from Northwest Europe for the period 1964-1988. (right) Same but for the western region of the USSR.

Ref.: M. Gadsden, A secular change in noctilucent cloud occurrence, *Journ. Atmos. Terr. Phys.*, **52**, 247-251. 1990.

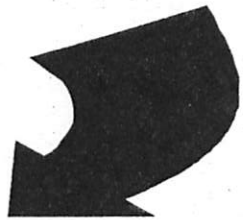
- Gadsden hypothesized a 7K cooling of the mesopause.
- Other evidence of mesospheric change
 - Lowering of Na-layer (Clemeshea, 1991)
 - Long-term decrease of temperature (0.5-1 K/yr at 70 km)
Hauchecorne et al (1991), Kokin and Lysenko (1994)
- Increase observed in OH temperatures in LT between 1980-91



Anthropogenic Forcings



Effects noticed to date

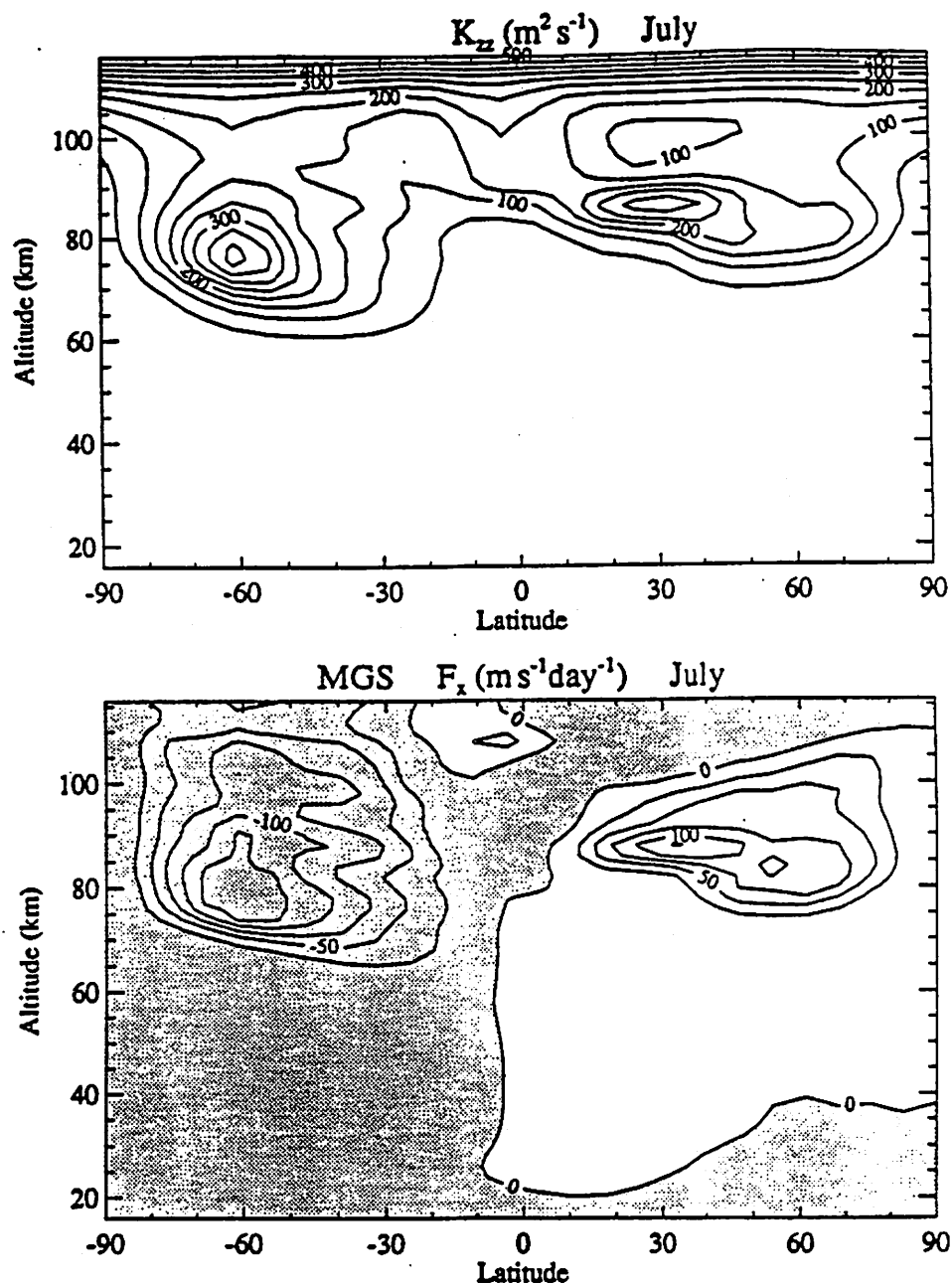


T-REX

Transition-Region EXplorer

? ?

Future Trends



Gravity wave forcing F_x (lower panel) and vertical eddy diffusion coefficient K_{zz} (upper panel) using the modified Garcia-Solomon 2D model. Ref: Portmann, R. W., The Heat Budget and Global Change in the Mesosphere, PhD Thesis, Univ. of Colorado, 1994.

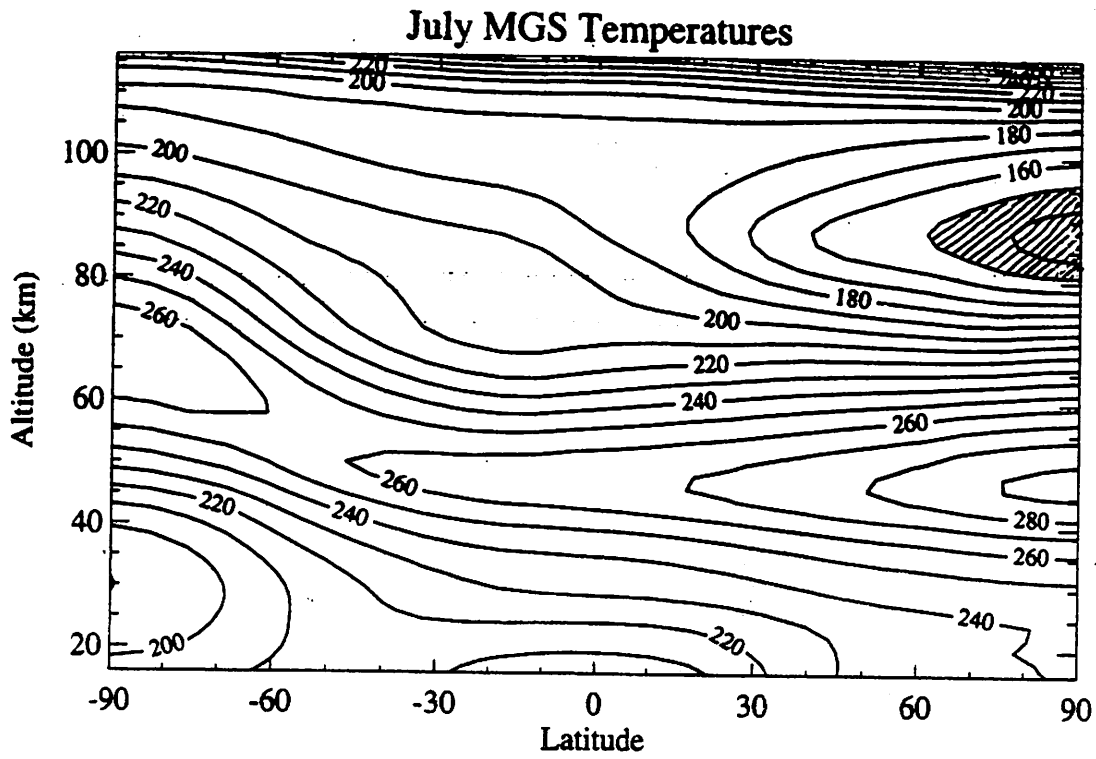
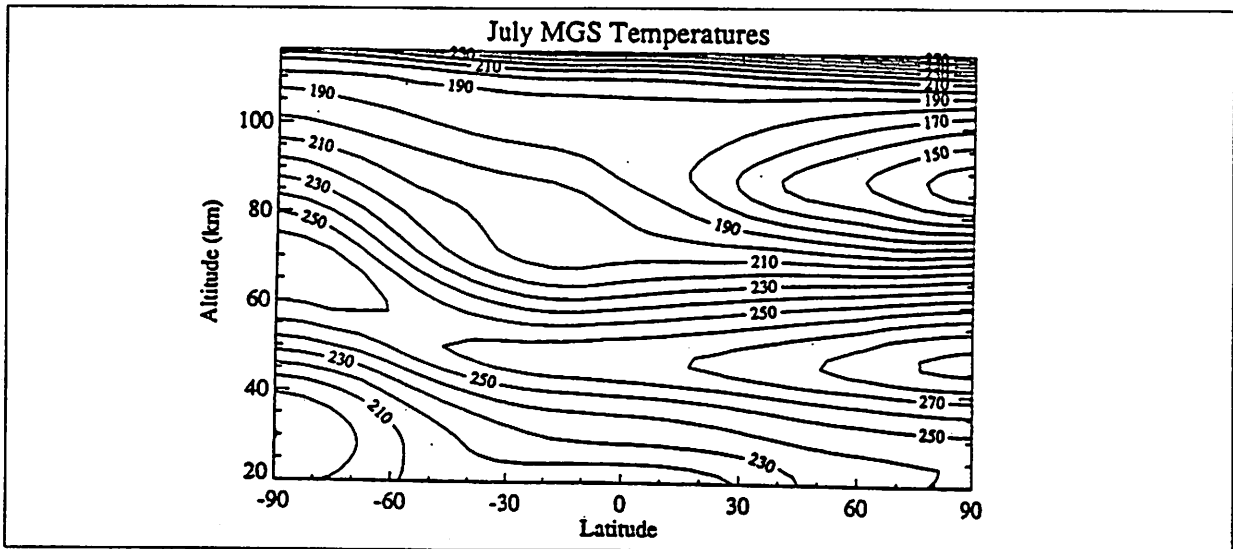
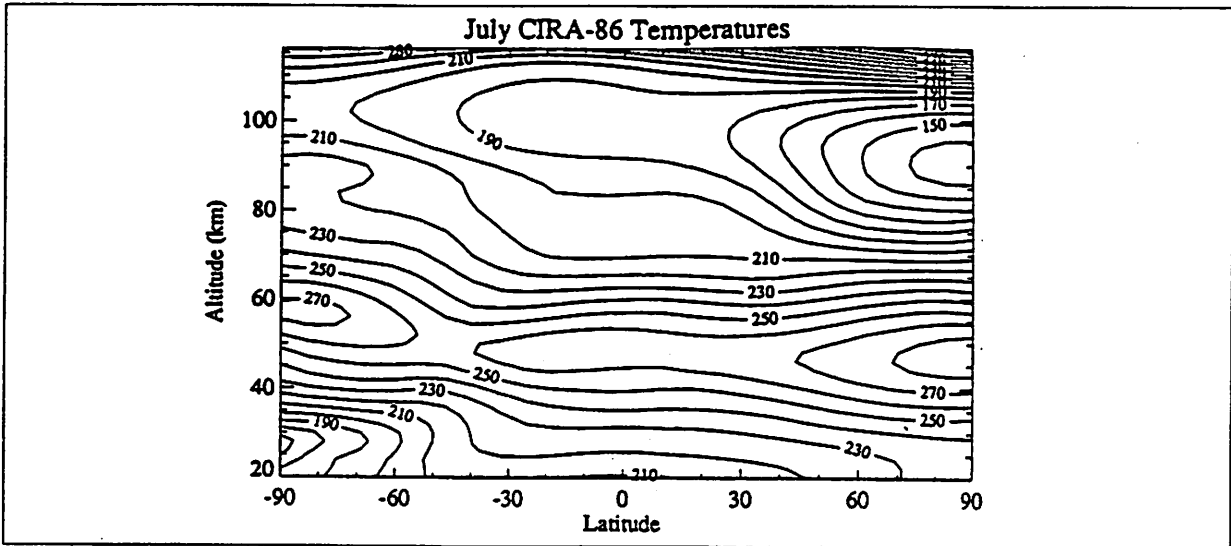
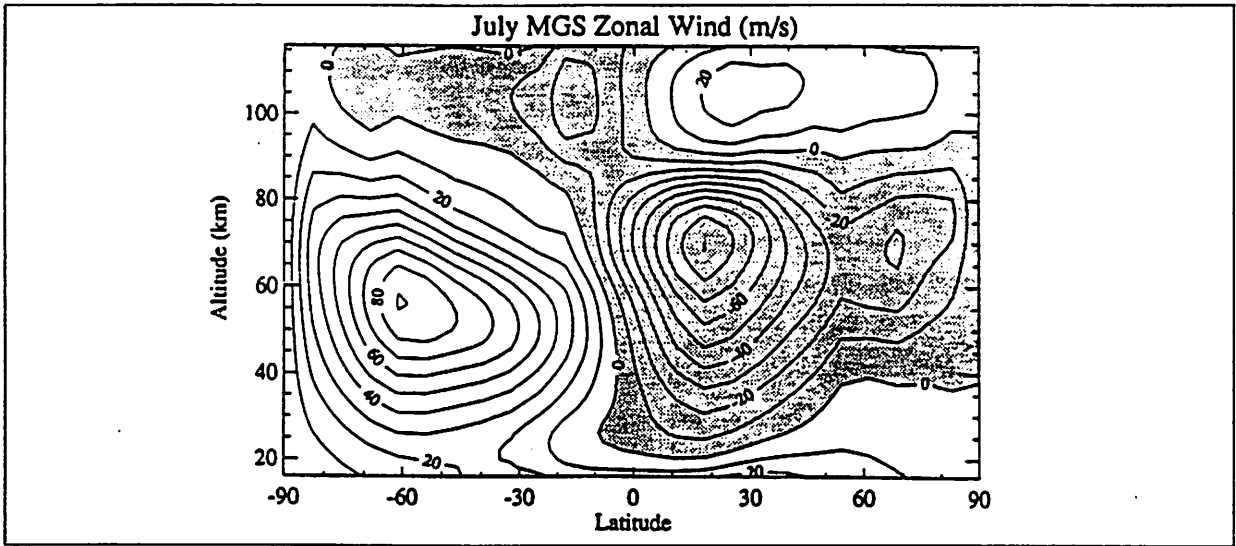
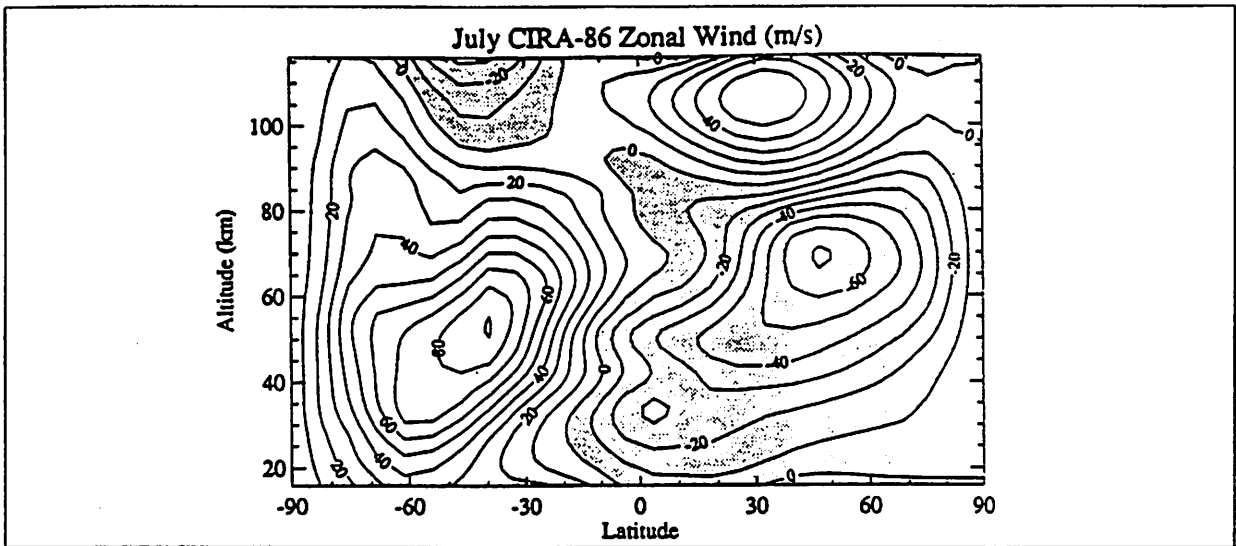


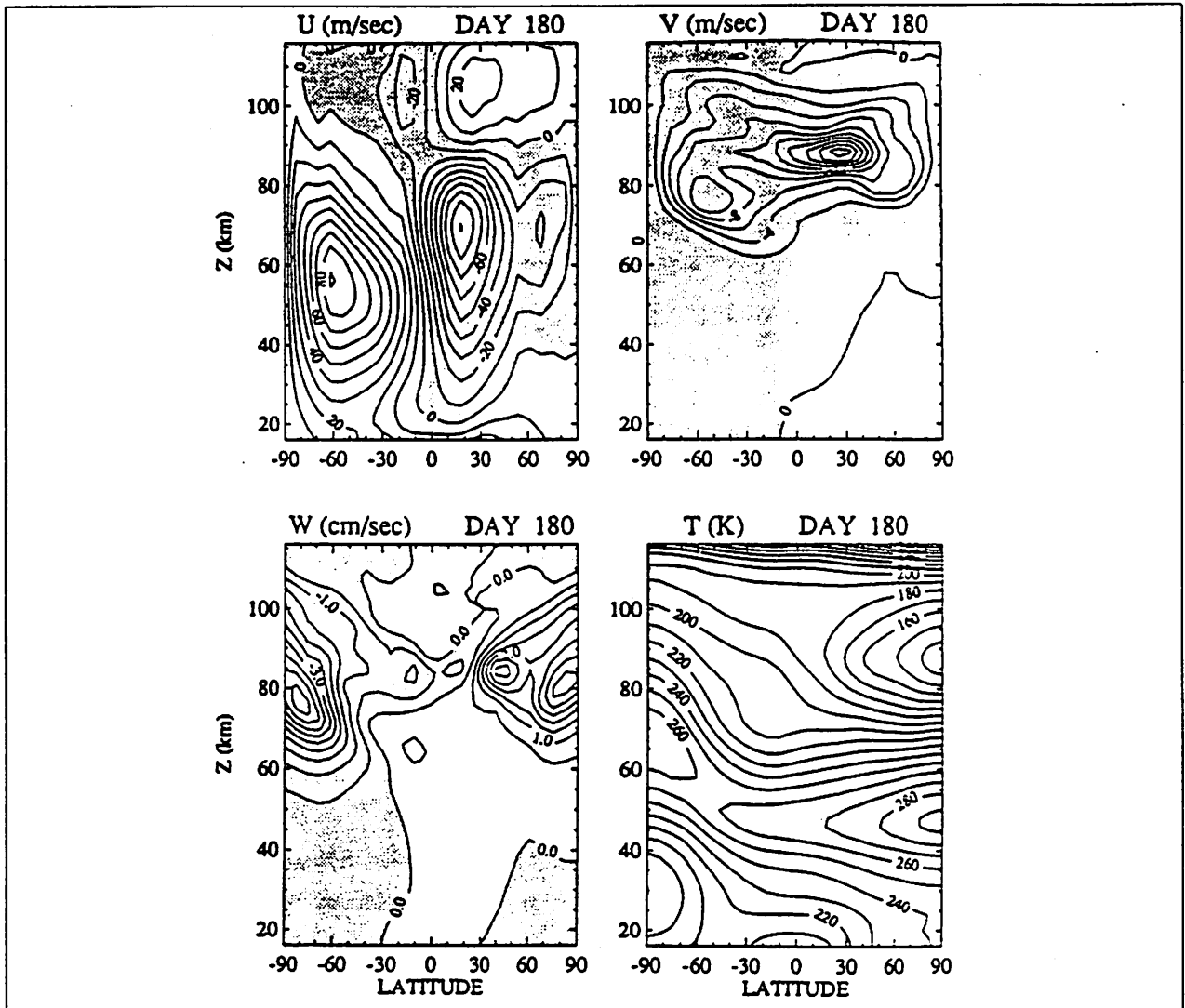
Figure 1. The zonal mean temperature field computed using the modified Garcia-Solomon (MGS) model for July. This model includes an improved diabatic heating calculation compared with Garcia and Solomon (1985).



(top panel) July temperature for the CIRA-86 model.
 July temperature for the modified Garica-Solomon model. $Pr=1$.
 From Portmann, 1994.



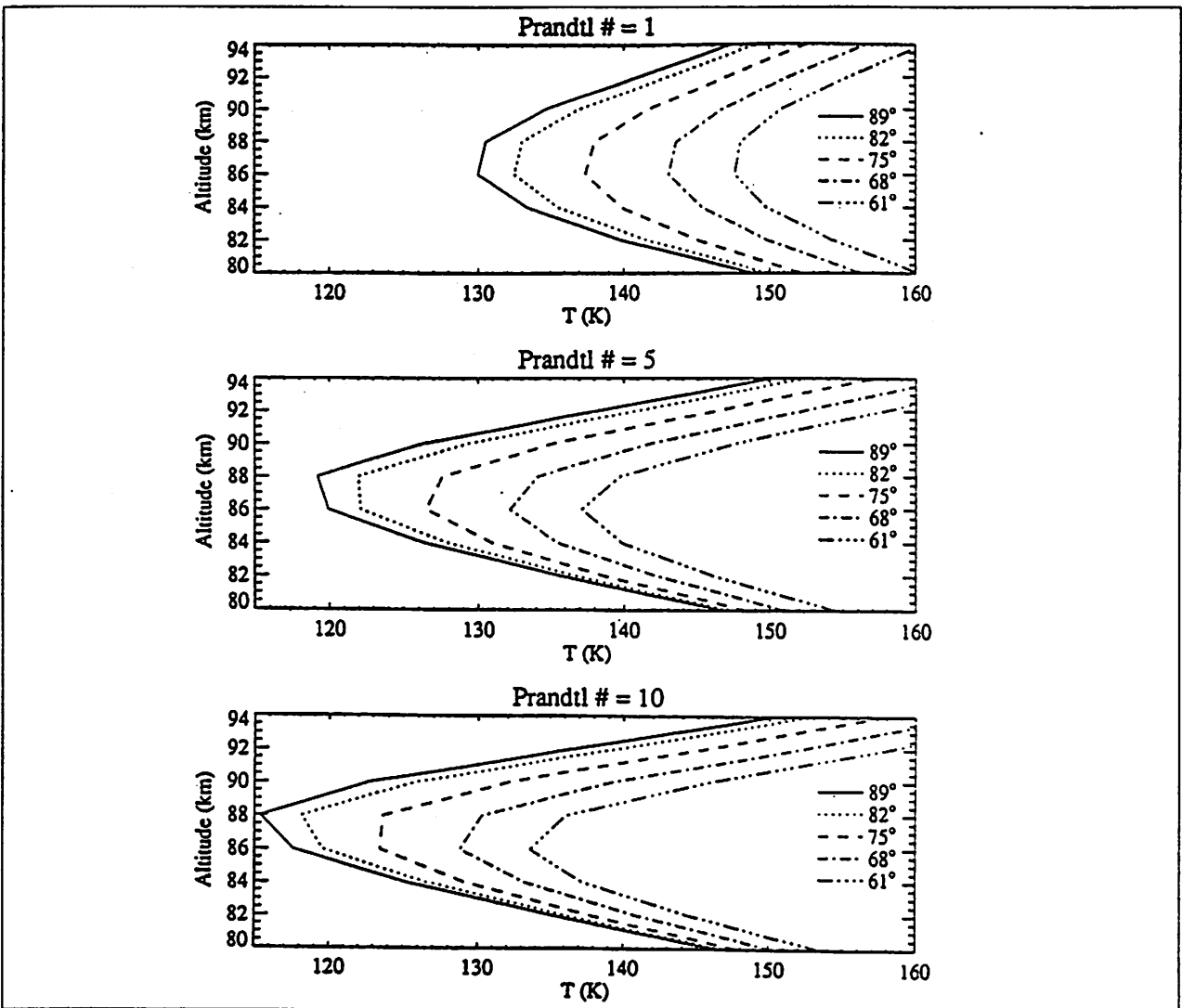
(top panel) July zonal wind for the CIRA-86 model.
July zonal wind for the modified Garica-Solomon model. Pr=1.
From Portmann, 1994.



Dynamical variables in the modified Garcia-Solomon 2D model.

- U is the zonally-averaged zonal wind velocity (positive toward west).
- V is the zonally-averaged meridional wind velocity (positive toward the pole).
- W is the zonally-averaged upward wind velocity (positive upwards).
 T is temperature in K. July conditions. Prandtl number=1.
 Negative regions are shaded.

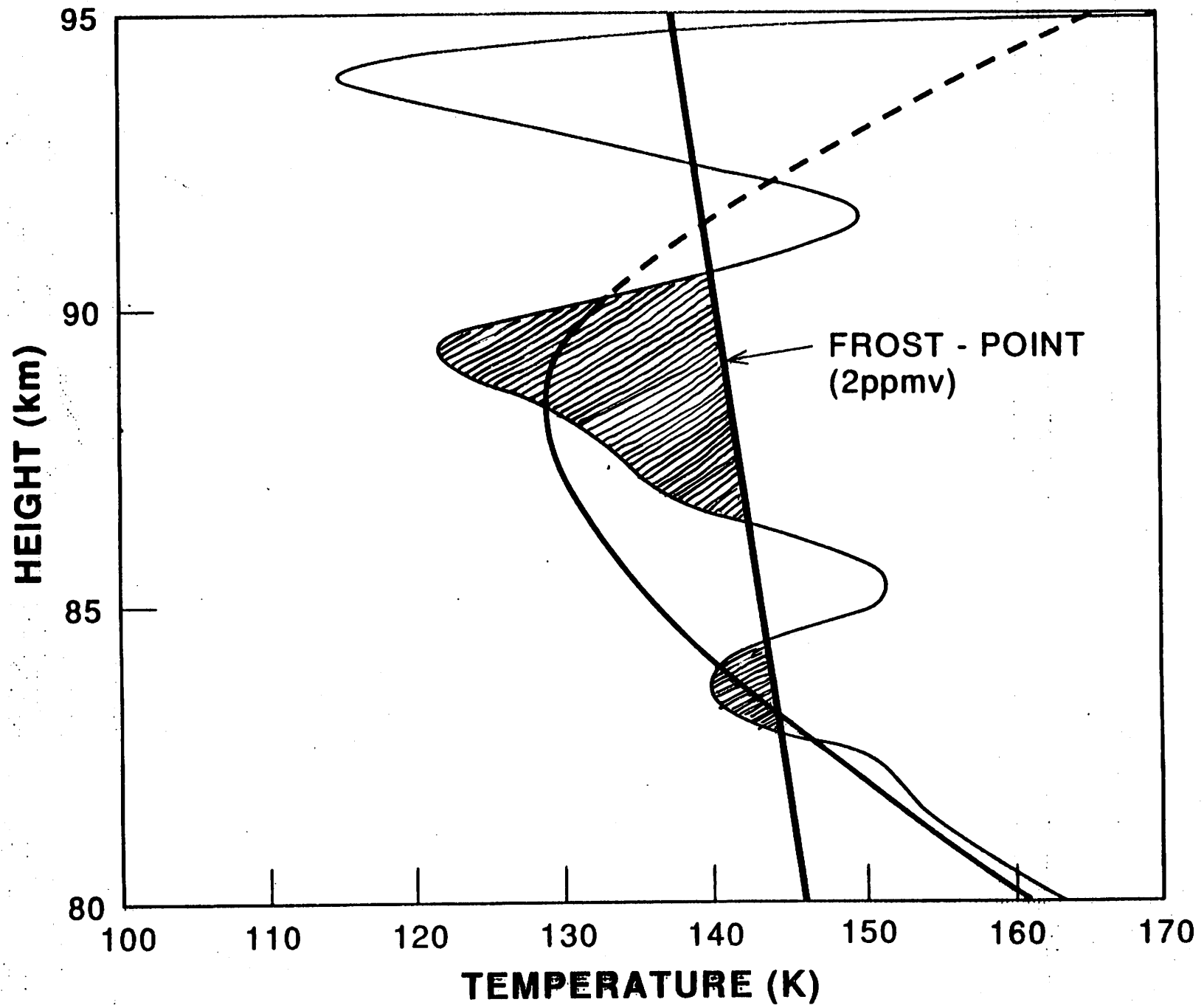
From Portmann, 1994.

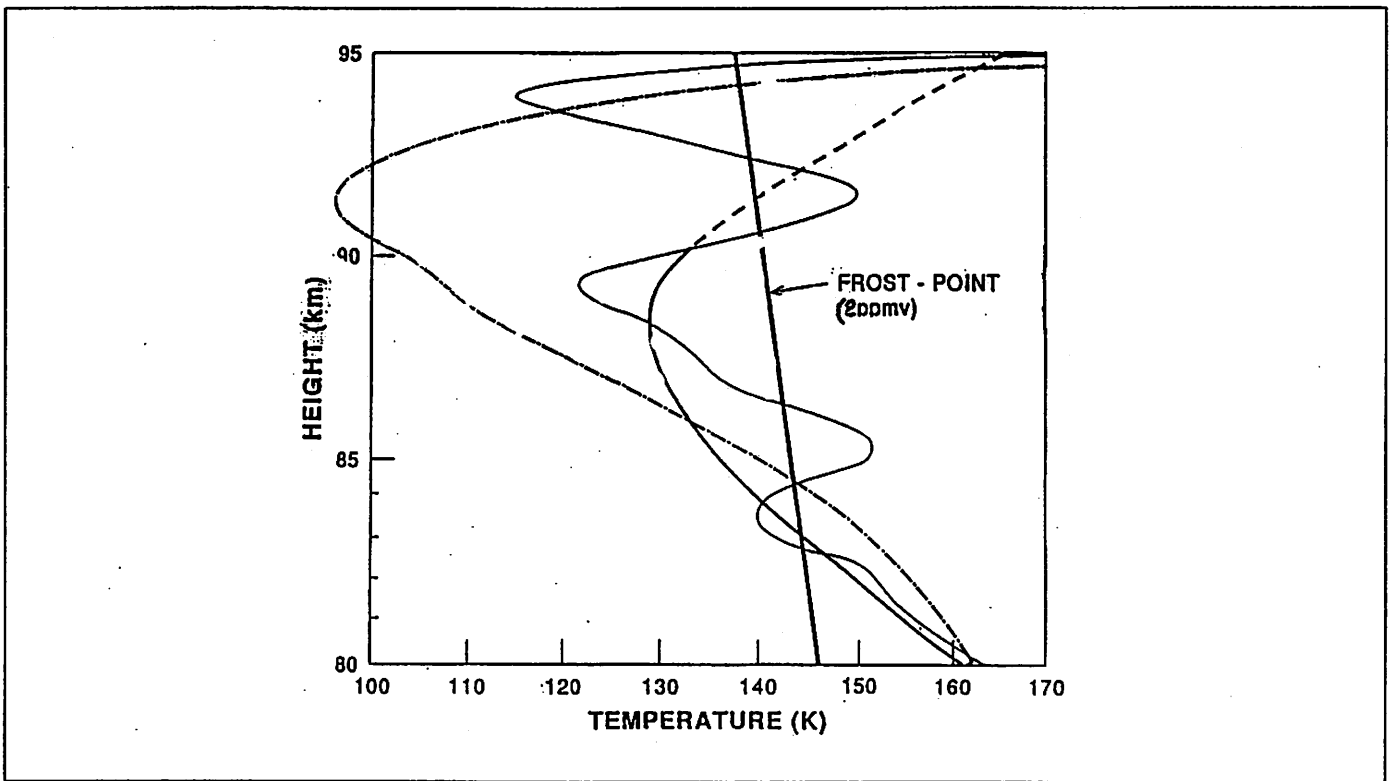


July temperature (K) profiles for the modified Garcia-Solomon 2d model. Different curves apply to different latitudes. Prandtl number (Pr) is the ratio of the eddy diffusion coefficient to the heat diffusion coefficient. From Portmann, 1994.

- As heat diffusion becomes less important (Pr increases) the mesopause temperature decreases.
- Prandtl numbers near 5 provide the best comparison with observation

Figure 3





Plot of high-latitude summertime temperature soundings derived from falling-sphere techniques (A): from Fritts et al., 1989 and (B) from Schmidlin, 1993. Plot C is an average of 30 soundings (June-August), from Lübken, F.-J. and U. von Zahn 1991.

- Water-ice crystals are stable in regions where the partial pressure of water exceeds the saturation water vapor pressure.
- Degree of Saturation, $S = \frac{\text{actual partial pressure of } H_2O}{\text{saturated vapor pressure}}$
- $S = \frac{n(H_2O)kT}{\exp[28.548 - 6077.4/T]} = \frac{w(H_2O)p(N \cdot m^{-2})}{\exp[28.548 - 6077.4/T]}$
- Frost point: Temperature for which $S=1$: At 86km ($p_{tot} = 0.00417 \text{ mb}$),

$$\text{and } T_f(K) = \frac{6077.4}{43.238 - \log_e[w(H_2O)]} \quad \text{where } w(H_2O) \text{ is in ppmv.}$$

Examples:

$w(H_2O)=1 \text{ ppmv}$ yields $T_f = 140K$.

$w(H_2O)=4 \text{ ppmv}$ yields $T_f = 145K$.

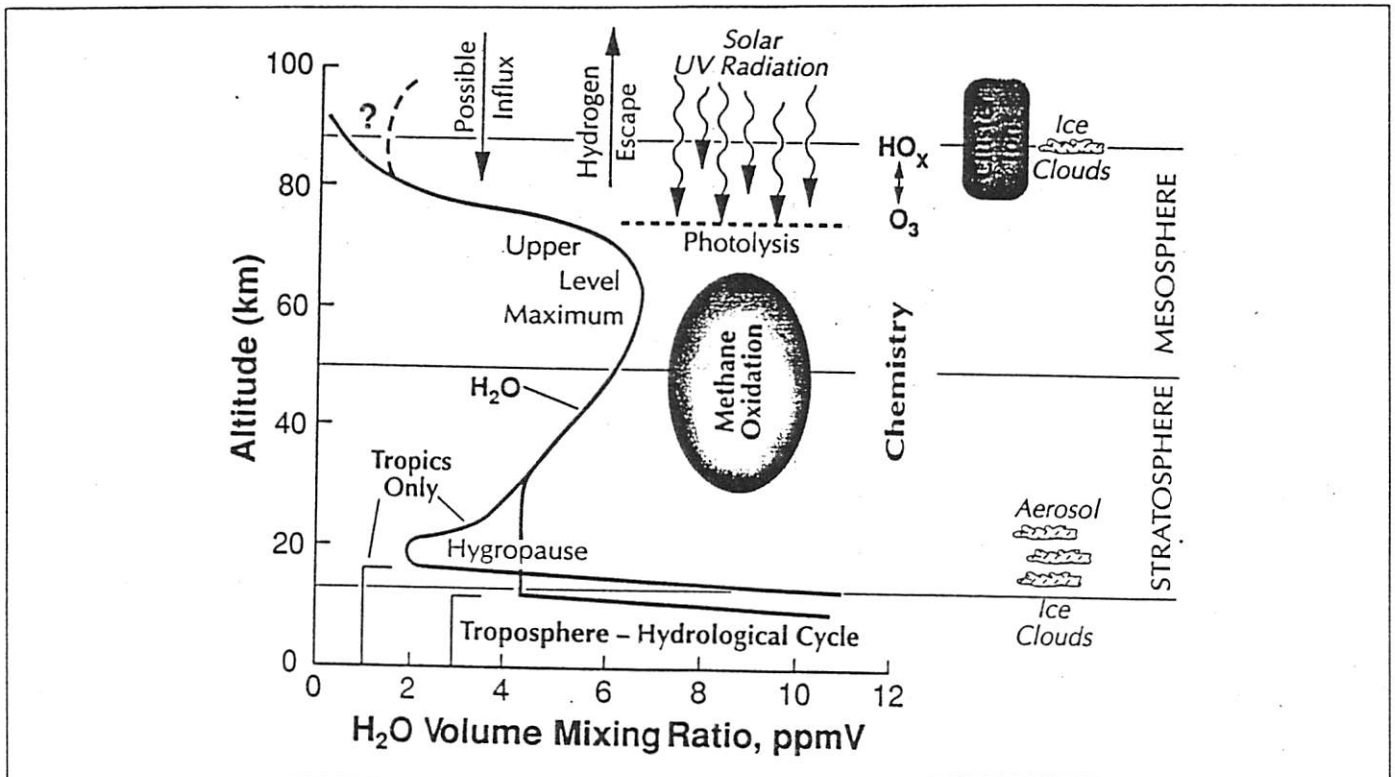
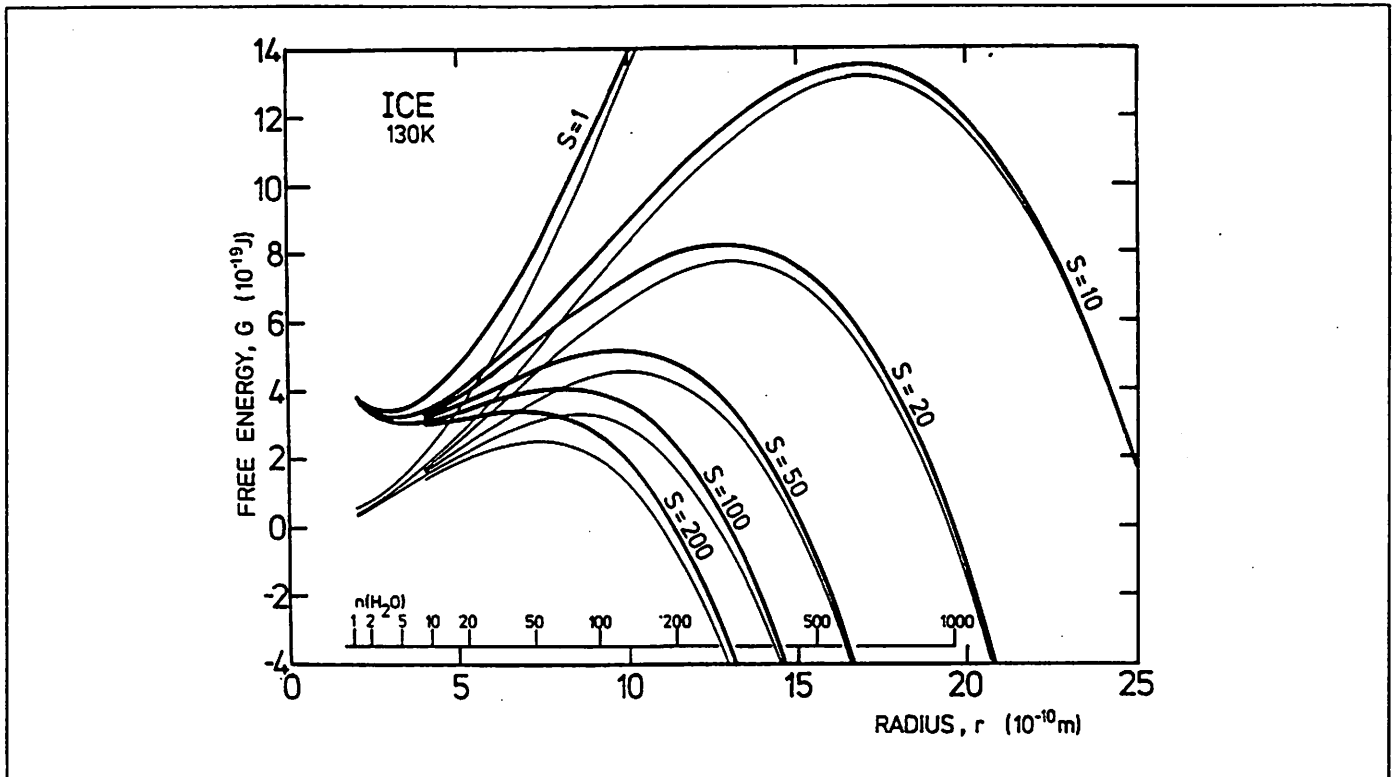


Illustration of the upper atmospheric water vapor budget.
 from Olivero, J.J., Water in the High Atmosphere, Penn. State Univ.,
 1985.

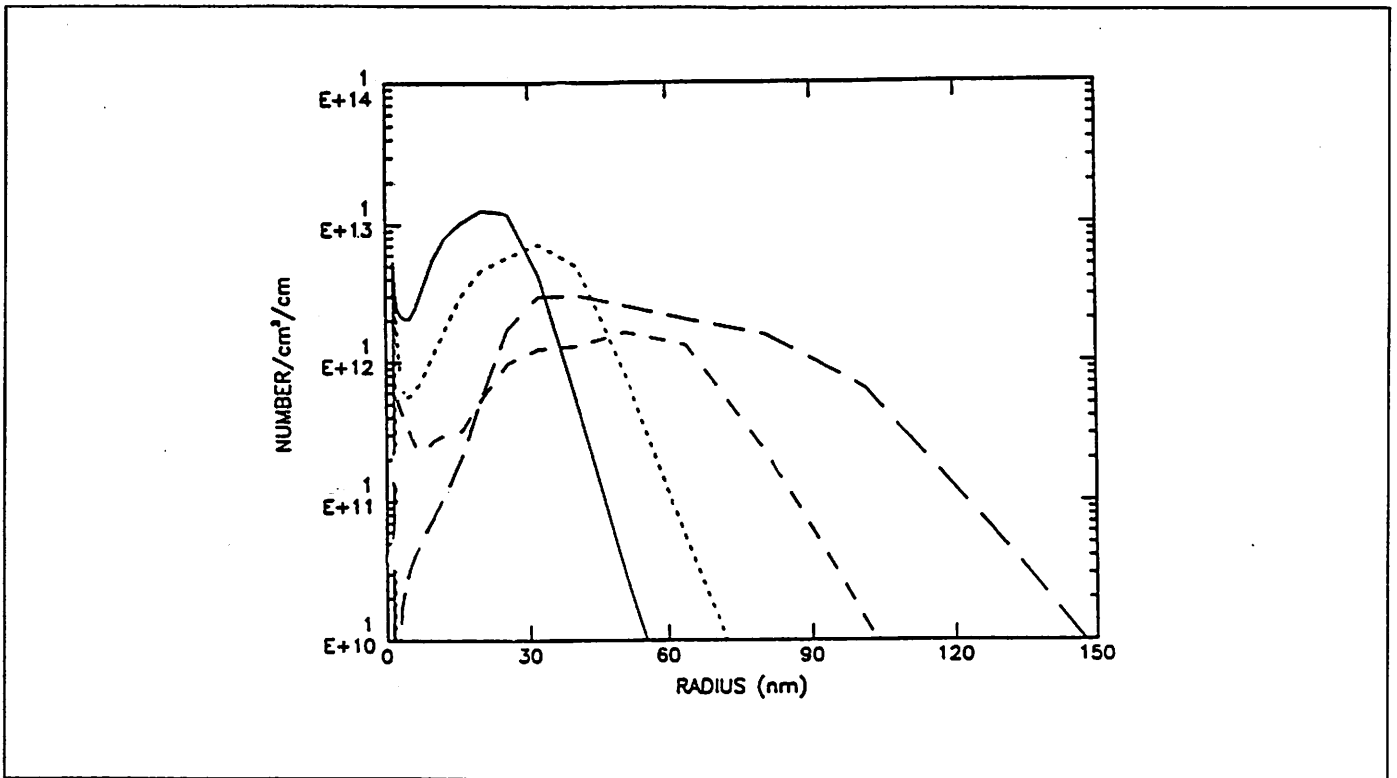
- The upper atmosphere is exceedingly arid, due to "freeze-drying" at the tropopause. About 50% of H_2O is from methane oxidation.
- Above ≈ 75 km, solar UV (primarily Lyman- α) dissociates H_2O
- Despite the dryness the upper atmosphere is super-saturated in two polar regions:
 - in the lower stratosphere in winter (Polar Stratospheric Clouds or PSC)
 - in the upper mesosphere in summer (Polar Mesospheric Clouds or PMC)



Calculated free-energy barriers governing the growth of an ice crystal for various saturation ratios S . The heavy lines are for growth around a singly-charged ion, the *lighter* lines for uncharged (homogeneous) nucleation. The scale at the bottom gives the number of H_2O molecules in the crystal at the indicated size.

From Gadsden and Schroder, *Noctilucent Clouds*, Springer-Verlag, 1989.

- **Nucleation:** - creation of embryo particles which exceed a certain size r_c necessary for accretional growth.
- From the diagram, we find for $S \approx 1$, growth occurs only for very large particles.
For $S = 10$, $r_c = 17 \text{ nm}$, $S = 20$, $r_c = 12 \text{ nm}$, $S = 50$, $r_c = 10 \text{ nm}$
- Growth rate is $dr/dt \propto (S - 1)$
- Sedimentation rate, $W_s \propto r$, where r is the particle radius

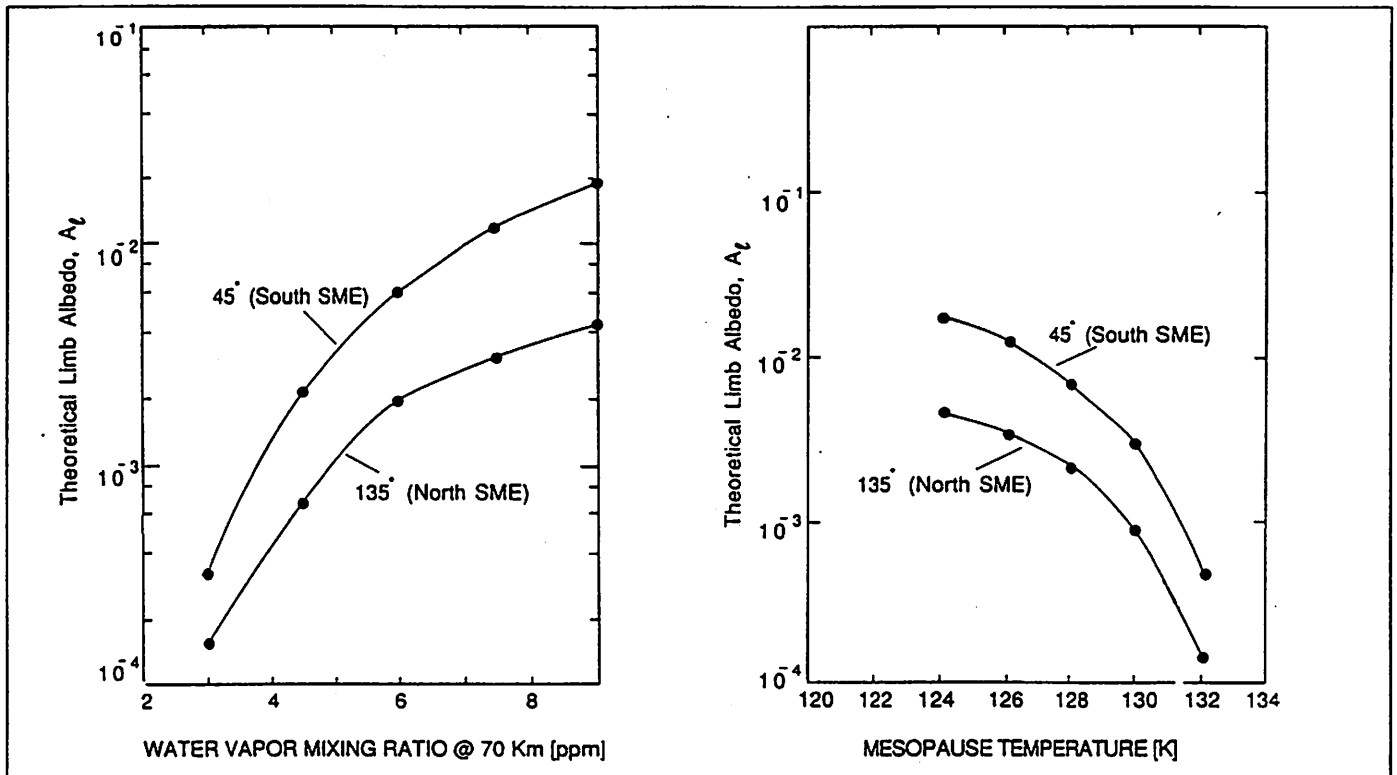


Particle size distributions $n(r)$ calculated by the aerosol model of Jensen et al, 1989.

- Model assumes **heterogeneous nucleation** from the meteoric dust distribution of Hunten et al. 1980.
- Consistent with UV measurements made by the SME UVS instrument.
- The scattered light intensity is given by

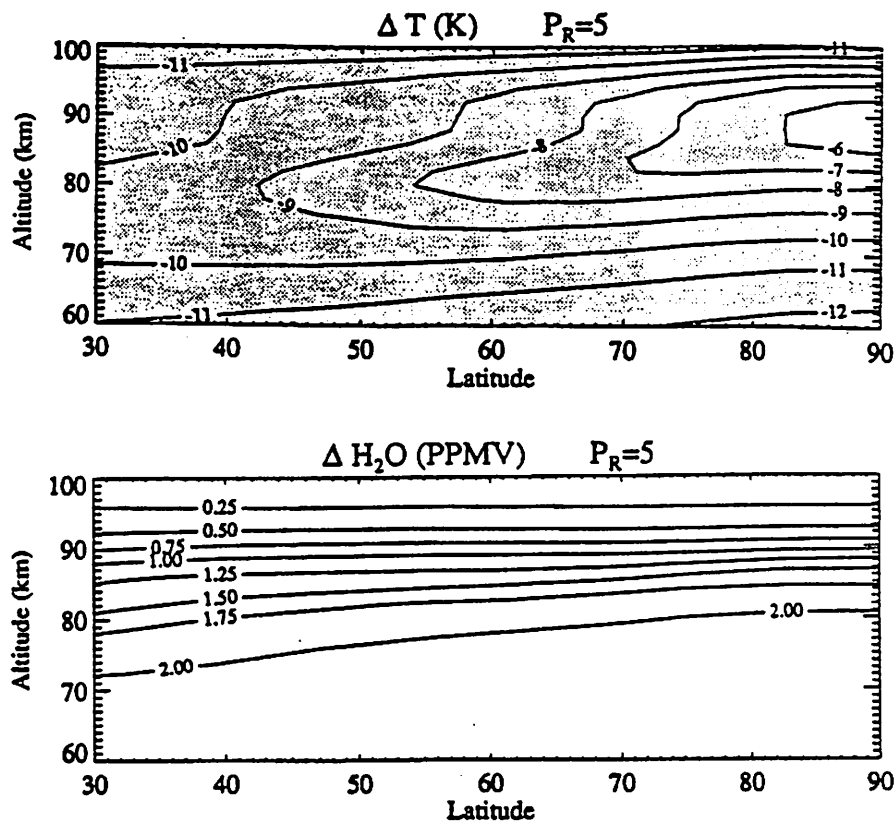
$$\text{Intensity} \propto \int_0^{\infty} dr n(r) r^m \quad (r < 100 \text{ nm})$$

- The power m is between 5 and 6, a very powerful dependence on particle radius.



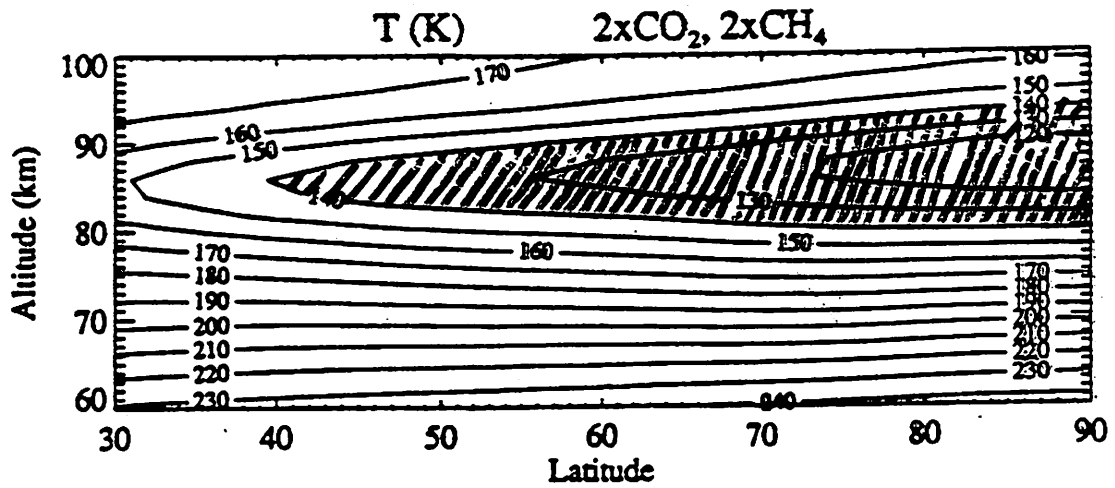
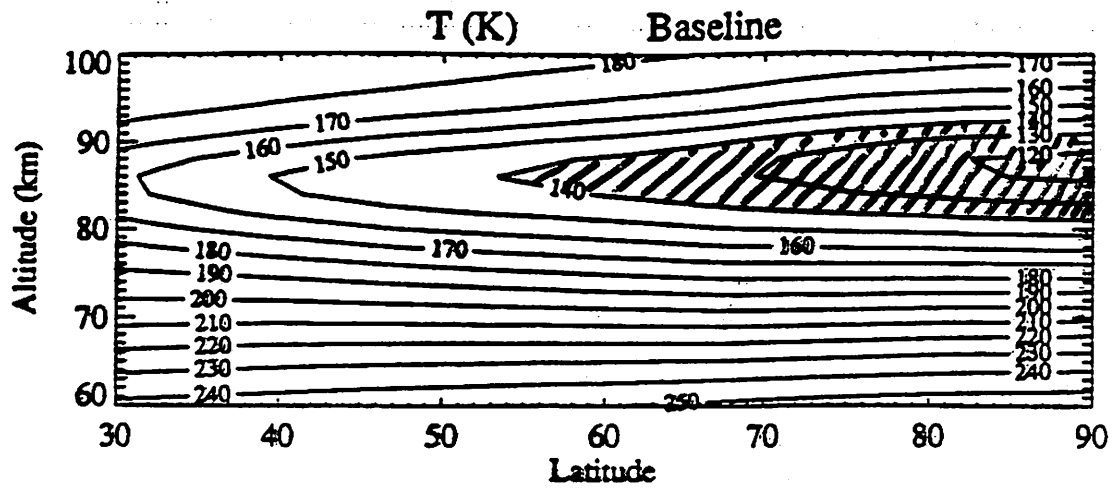
Theoretical limb brightnesses of PMC as seen from an orbiting spacecraft. The model of Jensen et al, 1989 was calculated for a nominal mesopause temperature of 128K (left panel), and for a nominal H_2O mixing ratio of 6 ppmv at 70 km (right panel). The scattering angles are appropriate for SME viewing in the northern and southern hemispheres.

- These diagrams illustrate the importance of H_2O and T in determining the scattered radiance of PMC.
- The Rayleigh-scattering background is 1×10^{-3}
- Both H_2O and T have natural variabilities of dynamical and solar origin, as well as from long-term anthropogenic causes



Calculated change in temperature and H_2O mixing ratio due to a doubling of CO_2 and CH_4 in the high-latitude summer mesopause (HLSM) region. Negative values are shaded. A Prandtl number of 5 was chosen to yield consistency with present-day mesopause temperature. From Portmann, 1994.

- The temperature was modeled in a self-consistent way, including radiative and dynamical feedbacks in the modified Garcia-Solomon 2D model.
- Temperature is lowered by 5 to 10K throughout the middle atmosphere
- H_2O at the HLSM is enhanced by $\approx 25\%$ due to enhanced CH_4 oxidation.



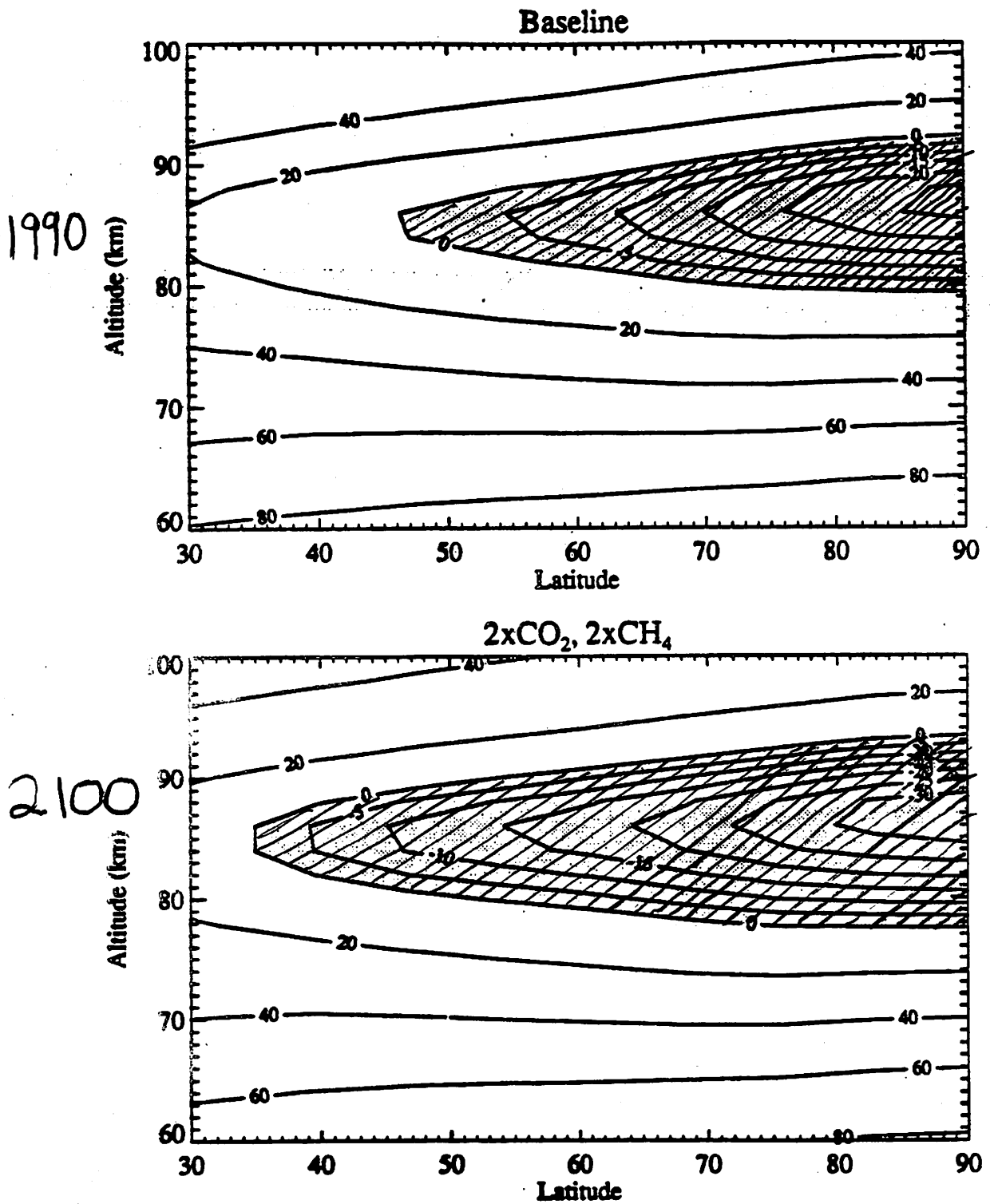
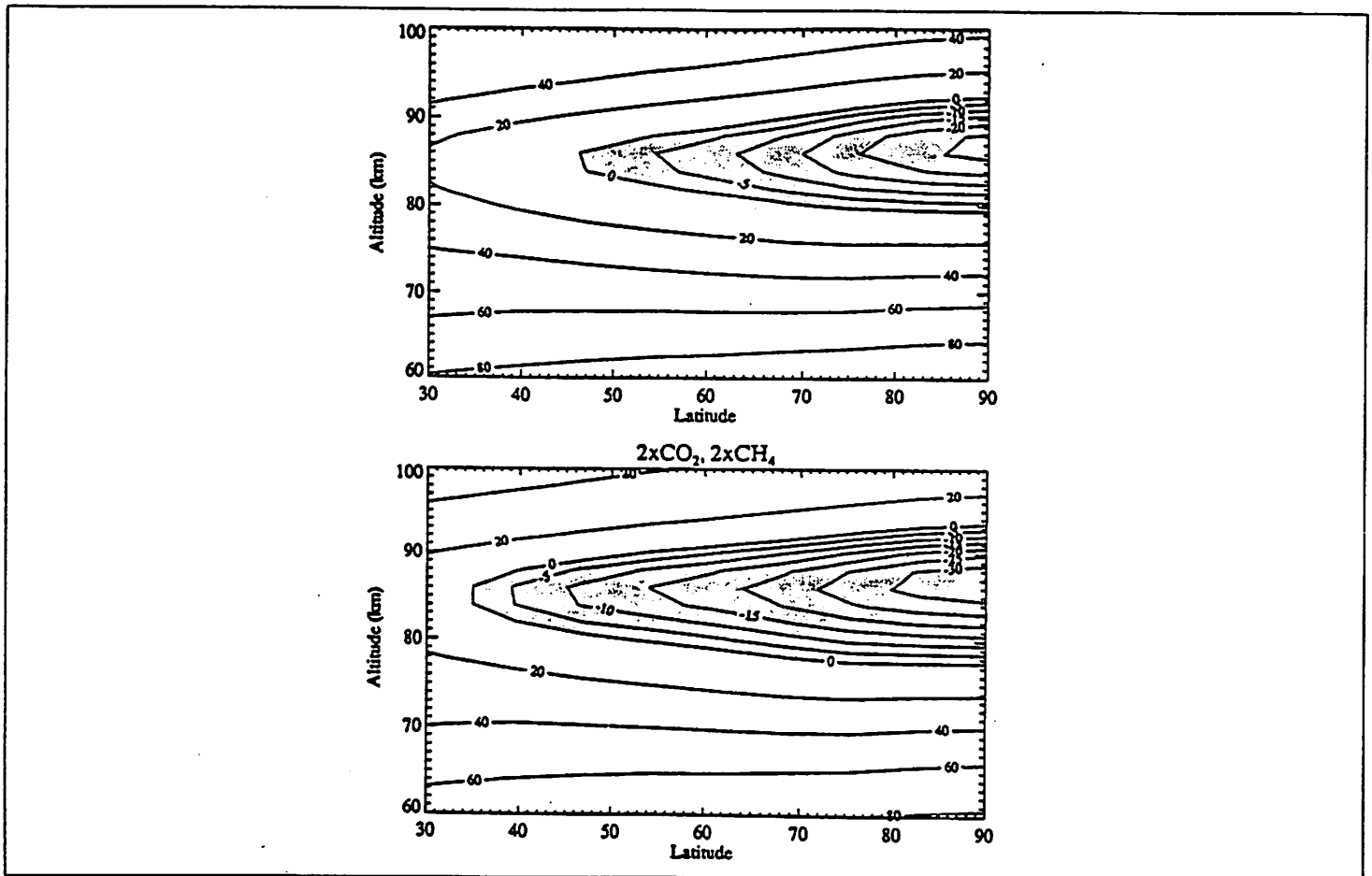


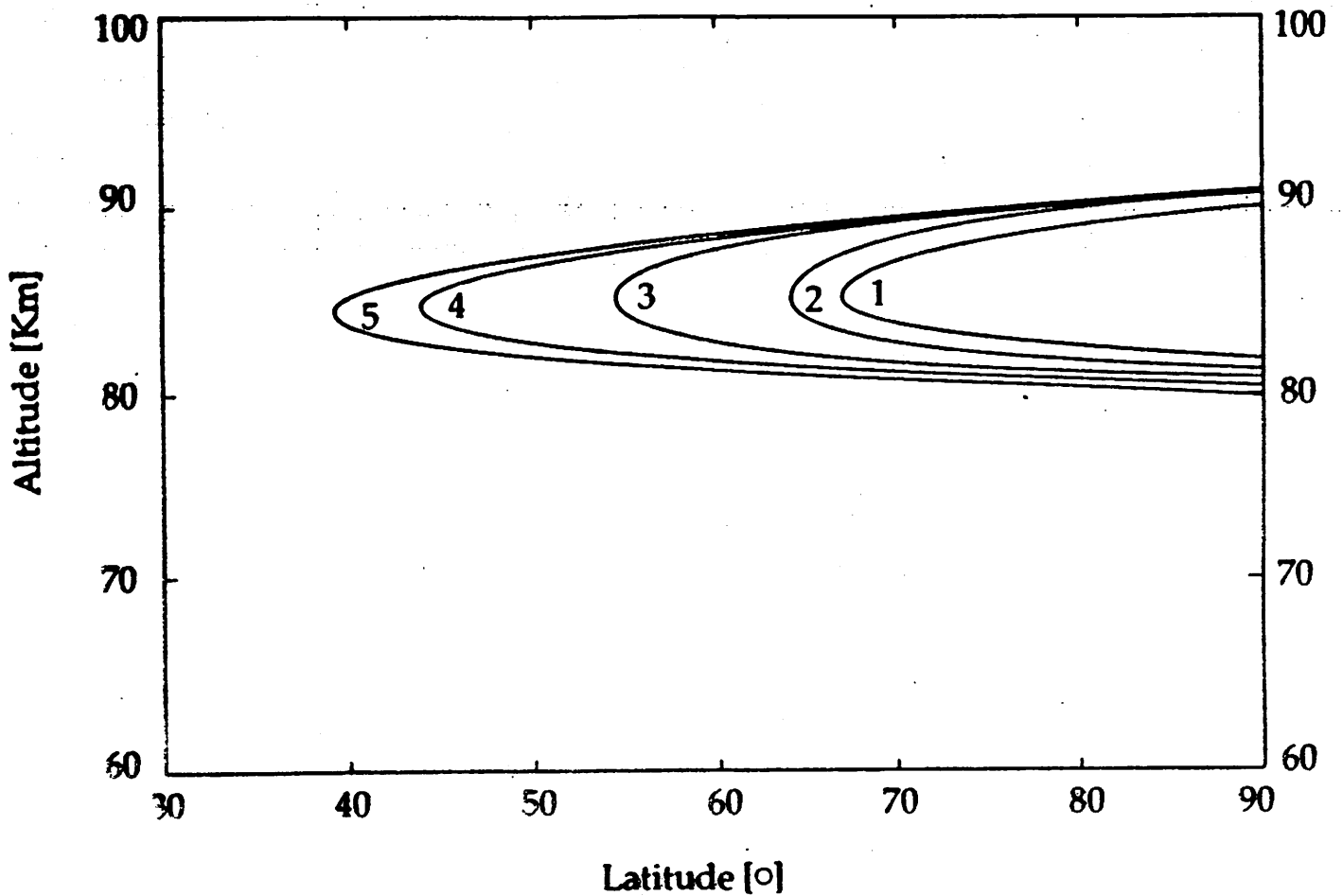
Figure 5-12 The degree of supersaturation of water vapor defined by the atmospheric temperature minus the saturation temperature for the baseline and doubled CO₂ and CH₄ atmosphere in July. The existence region of ice particle growth (i.e., negative values) are shaded.



Calculated water-ice existence region defined as the contour of constant saturation ratio S . Upper panel: present-day conditions. Bottom panel: Doubled- CO_2 , CH_4 scenario. $Pr=5$. From Portmann, 1994.

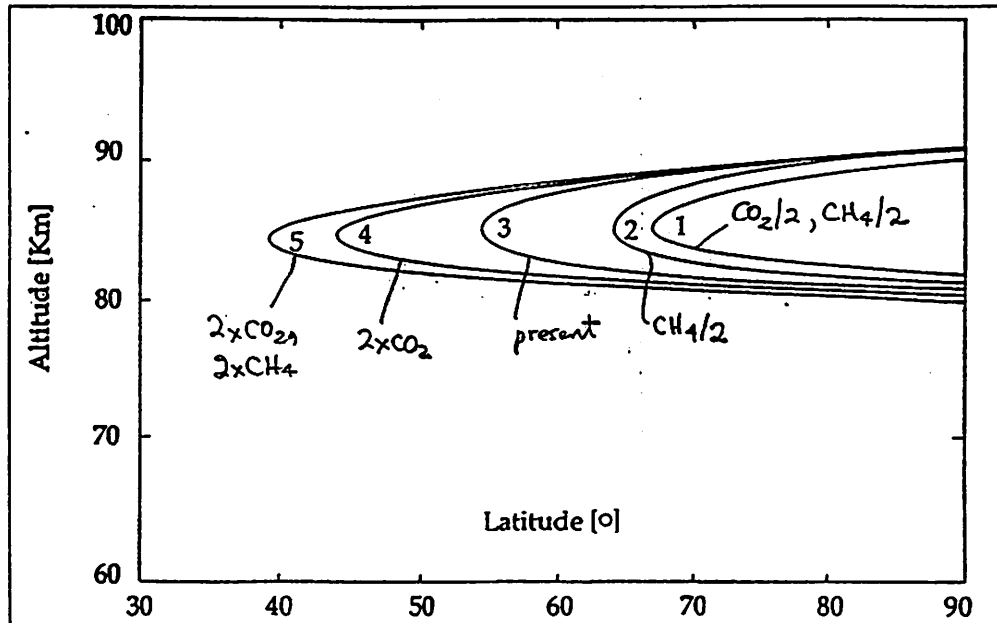
- The present-day ice existence region extends to about 45° latitude, too far equatorward to agree with the NLC boundary, known to be at about 50° latitude.
- Hypothesis: ice clouds form when $S > 5, T < 145K$, on the average.
- An actual ice cloud probably forms in still colder pockets of air $T < 130K$, as a result of adiabatic cooling as occurs in e.g. small-scale internal gravity waves

Contours of Cloud Existence Region



Scenario	Date/Epoch	CO ₂ (ppmv)	CH ₄ (ppmv)	Ice existence latitude boundary
1	Glacial	165	0.75	67°
2	1895	290	0.9	63°
3	present	330	1.5	55°
4	late 21-st century	660	1.5	45°
5	late 21-st century	660	3.0	39°

Table 1. Five scenarios for past and future middle atmosphere climate simulations. Latitude boundary is defined by the most southerly latitude where the frost point is -5K below the ambient temperature.

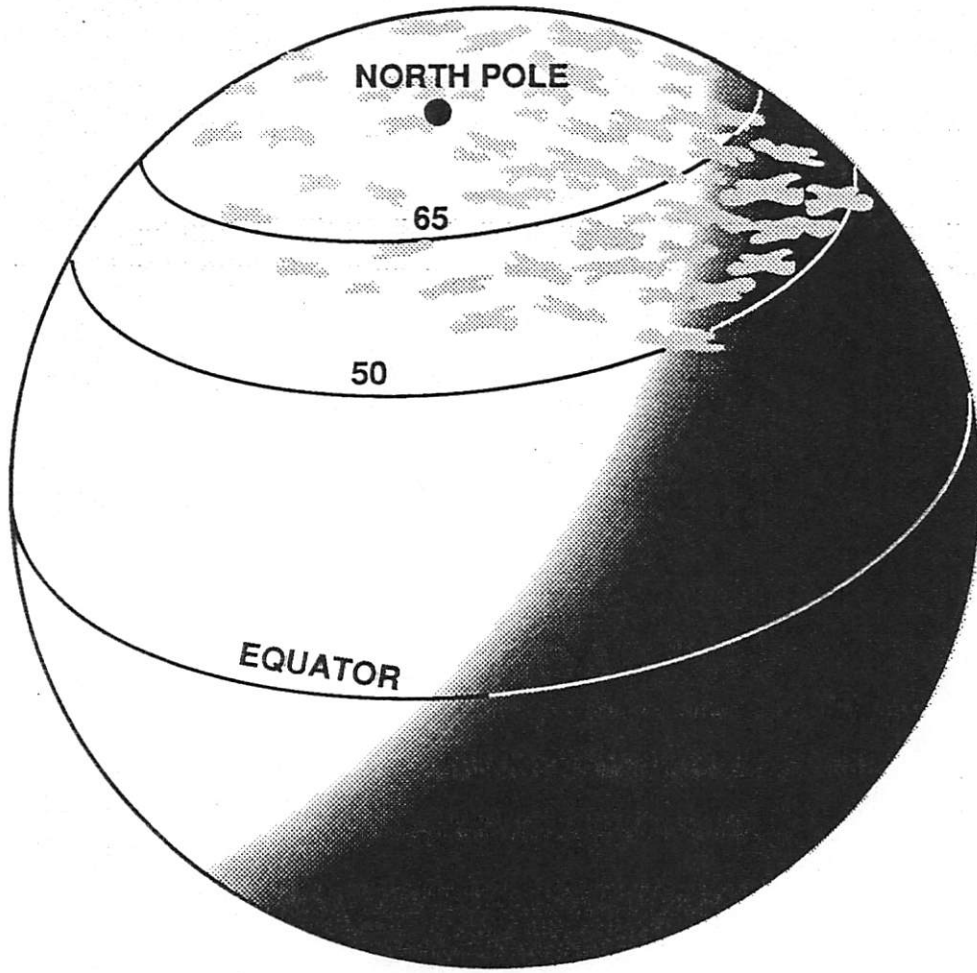


Contours of ice-cloud existence region ($S=5$) calculated from the 2D model for five scenarios, given in the table below. $Pr=5$. From Portmann (private communication, 1994)

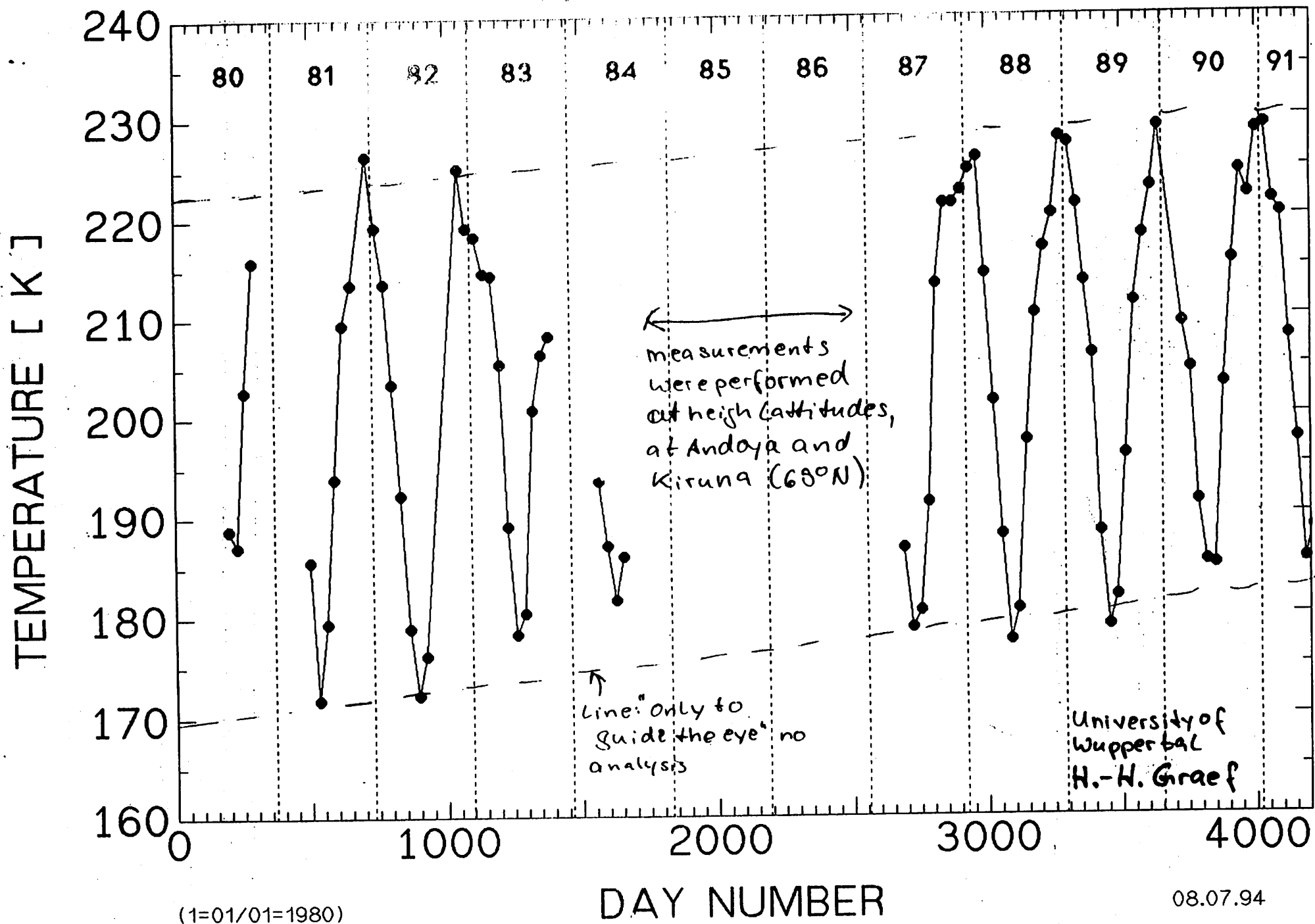
Scenario	Date/Epoch	CO ₂ (ppmv)	CH ₄ (ppmv)	Ice existence latitude boundary
1	Glacial	165	0.75	67°
2	1895	290	0.9	63°
3	present	330	1.5	55°
4	late 21-st century	660	1.5	45°
5	late 21-st century	660	3.0	39°

Five scenarios for past, present and future middle atmosphere climate simulations, based on the data and “business-as-usual” predictions given in *Intergovernmental Panel on Climate Change*, 1990.

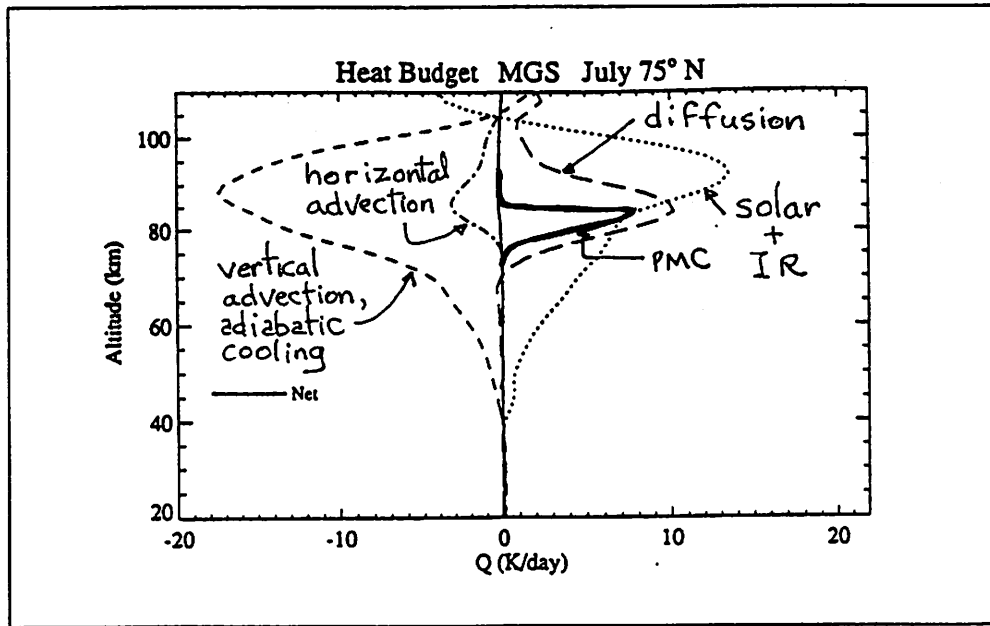
- Pre-1885, the model shows that NLC were northward of 60° latitude.
- Increasing levels of CO_2 lower the temperature, while increasing CH_4 raise the humidity. This causes equatorward advance of the NLC zone.
- In the future, if trends continue, NLC should advance still farther into more populated areas at temperate latitudes.



Wuppertal (51°N/7°E)

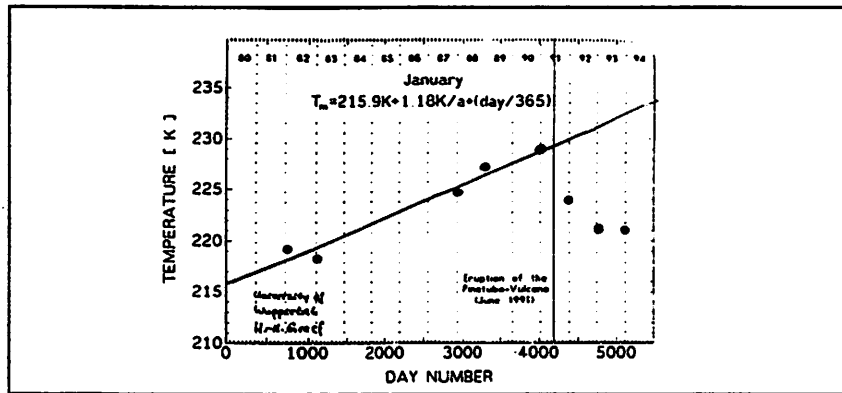


Recent Research

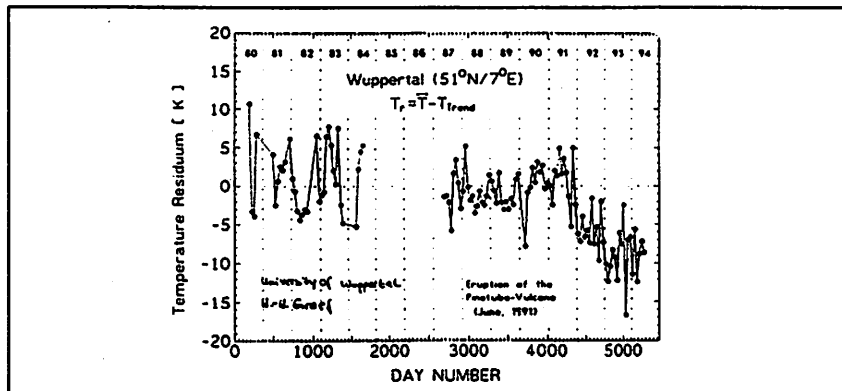


Components of the heat budget at the HLSM, calculated from the 2D model. Also shown is the heating rate due to the absorption of solar and IR terrestrial radiation from a very bright NLC. From a calculation by E. J. Jensen (private communication, 1995)

- Heating of the atmosphere by ice particle absorption was previously unrecognized as an important component of the HLSM heat budget. The heating rate is \propto to the visible optical depth τ of the cloud.
- This may provide an important *self-limiting* mechanism on the particle size.
- Brighter clouds \rightarrow more heating \rightarrow higher temperature \rightarrow sublimation of ice, and \rightarrow destruction of ice cloud.
- Possible Implications: medskip
 - Explains current-day upper limit on τ of PMC.
 - Reduces or eliminates the impact of increased CO_2 , CH_4 on τ .
 - Current τ no longer provides a useful upper limit on small-comet flux of H_2O (Jensen and Thomas, 1988).



Yearly-averaged temperature measured by the ratios of rotational lines in the (3,1) OH Meinel band. Effective height and thickness is at 86 km and 10 km, respectively. The straight line is the best-fit linear trend, for data prior to 1991. Significant cooling followed the Mt. Pinatubo volcanic eruption in June, 1991. Ref: H.- H. Graef and D. Offermann, Decrease of mesopause temperatures after the eruption of Mount Pinatubo, Middle Atmosphere Symposium, IAMAP, 1993.



Temperature residuals (temperature less the long-term trend) versus time. The small-scale oscillations ($\approx 50K$ peak-to-trough) are due to an annual temperature cycle (higher in winter and lower in summer).

- Pre-1991 trends for both Wuppertal (51°N) and Kiruna (69°N) are similar, $dT/dt \approx +1K/yr$. *This is opposite to the CO₂ cooling effect predicted by models!*
- Also why should a volcanic eruption cool the mesopause region? Could this have happened following the Krakatoa eruption in 1883, giving rise to bright NLC displays in 1885?